EFDA–JET–PR(10)28

R. González de Orduña, M. Hult, G. Bonheure, M. Laubenstein, G. Marissens,
P. Vermaercke J.S.E. Wieslander, A. Murari
and JET EFDA Contributors

# Monitoring the Leakage of 3.0MeV and 14.7MeV Protons from a Fusion Plasma

# Monitoring the Leakage of 3.0MeV and 14.7MeV Protons from a Fusion Plasma

R. González de Orduña[1], M. Hult[1], G. Bonheure[2], M. Laubenstein[3], G. Marissens[1], P. Vermaercke[4], J.S.E. Wieslander[1], A. Murari[5]
and JET EFDA contributors*

***JET-EFDA, Culham Science Centre, OX14 3DB, Abingdon, UK***

*[1]EC-JRC-IRMM, Institute for Reference Materials and Measurements, 10 Retieseweg 111, B-2440 Geel, Belgium*
*[2]Laboratory for Plasma Physics, Association "Euratom-Belgian State", Royal Military Academy, Avenue de la Renaissance, 30, Kunstherlevinglaan, B-1000 Brussels, Belgium*
*[3]17 Laboratori Nazionali del Gran Sasso, I.N.F.N. 18 S.S. 17/bis, km 18+910, I-67010 Assergi (AQ), Italy*
*[4]Studiecentrum voor Kerenergie • Centre d'Etude de l'énergie Nucléaire, SCK•CEN, Boeretang, B-2400 Mol, Belgium*
*[5]Association EURATOM/ENEA, Consorzio RFX, 4-35127 Padova, Italy*
** See annex of F. Romanelli et al, "Overview of JET Results", (Proc. 22[nd] IAEA Fusion Energy Conference, Geneva, Switzerland (2008)).*

Preprint of Paper to be submitted for publication in
Nuclear Instruments and Methods in Physics Research Section A

**ABSTRACT.**
An experiment to study, separately, the leakage of protons of 3.0MeV and 14.7MeV in the JET Tokamak, is presented. The activity of the activation products induced by the plasma in different samples that were placed inside the Tokamak was measured using Ultra Low-level Gamma Ray Spectrometry (ULGS). Stacking of some of the samples during activation allowed differentiating between the protons of 3.0MeV and 14.7MeV that originated in two different reactions in the plasma. For the B4C sample the ratio of the 3.0 and 14.7MeV proton flux could be determined as 0.17(10) assuming normal incidence and 0.31(16) assuming 45$^{o}$ incidence. For LiF the result obtained was that, within the uncertainty, there was no contribution from the 3.0MeV protons.

## 1. INTRODUCTION

The confinement time for a fusion plasma is mainly determined by the rate of loss of charged particles across the magnetic field. Charged particles in the MeV range are produced in large quantities in fusion reactions. The leakage of these particles is a potential hazard to the reactor walls and material structures that contain the fusion plasma. Because of the extreme conditions inside the JET Tokamak there is still no standard technique to analyse the leakage of charged particles from the plasma. The short range of these particles prevents any attempt to measure them outside the Tokamak walls, as it is done for neutrons. The most promising solution for retrospective studies is to place samples of different materials inside the Tokamak and afterwards analyse the activation products. This approach for studying the charged particles inside the JET Tokamak was carried out for the first time in 2004 [1]. A second experiment was carried out in 2006 [2-4] in which for the first time conclusive evidence of proton induced activity was discovered. The third experiment was carried out in 2008 and had three aims: (i) search for alpha particle induced reactions, (ii) determine the angular distribution of proton induce reactions and (iii) study the possibility of quantifying the relative amounts of protons with 3.0MeV and 14.7MeV. The first two points were described in a recent publication [5]. The aim of this paper is to describe the third part of the experiment from 2008.

The number of samples used in this experiment was forty-five. In order to measure the very low activities that were induced (in the order of mBq) it was essential to use ULGS and to measure each sample for a relatively long period of time (typically one week per sample). In order to measure relatively short-lived radionuclides (half-lives in the order of a few days), logistical issues and the access to many underground High Purity Germanium (HPGe) detectors was crucial

## 2. MATERIALS AND METHODS

### *2.1. EXPERIMENT AT JET TOKAMAK*

Forty-five samples of nine different materials were placed inside the JET Tokamak. Nineteen of these samples were placed in five stacks. Each of the stacks was of a different material: HAVAR (a cobalt based alloy), Lithium Fluoride (LiF), boron carbide ($B_4C$), rhodium (Rh) and yttrium (Y). The holder for these samples was a Boron Nitride (BN) probe with hexagonal cross section. Figure

1 shows (a) the cross section of the probe and its orientation with respect to the toroidal magnetic field ($B_t$) and the major radius of the tokamak ($R_{in}$). The numbers indicate the six slots where the samples could be placed. (b) A picture of the BN activation probe and (c) a schematic diagram of the sample layout. It was the same holder as was used in the experiments from 2004 and 2006 . The holder was hanging from the ceiling of the JET Tokamak. The distance from the tip of the probe to the plasma was 140mm. At each of the faces of the hexagonal holder was a slot in which to put the samples. The probe was 10cm long. Each slot was 1.0cm wide and could hold samples that were 1mm thick. The materials of the samples and probe were carefully selected to resist the harsh conditions inside the Tokamak and to obtain, after the exposure to the plasma, activation products that were gamma-ray emitters with half lives long enough to measure the activity in a reasonable time after the irradiation.

The number of samples in each stack and the thickness of them were different for each material. An overview of the thicknesses, length and masses of these samples is presented in Table 1. Note that vanadium foils (0.02mm thick and 5.0cm long) were used to cover all samples in slots 1, 3, 4 and 5 (at $0^o$, $120^o$, $180^o$ and $240^o$ with the internal radius, see Fig.1). The main aim with the vanadium foil was to detect alpha particles via the 51V($\alpha$,n)54Mn reaction, which was discussed in a recent paper [5]. No positive evidence of alpha particles could be detected. A main reason for this is the very low yield of this reaction at 3.6MeV.

For some of the samples that were not placed in stacks (TiVAl, Ti and V) a study of the angular distribution of the proton flux was carried out [5]. The conclusion of this study was that the flux of protons was at its maximum for the slots 1, 2 and 6 (at $0^o$, $60^o$ and $300^o$ with the internal radius, see Fig.1). It was significantly lower (about 2 orders of magnitude) for the other orientations. This angular distribution could later be obtained from computer calculations [6] and provided information on the behaviour of the plasma.

The other samples that were not placed in stacks, such as the LiF and B4C placed in the slots 2, 3 and 4 (at $60^o$, $120^o$ and $180^o$ with the internal radius, see Fig.1), were used to monitor the charged particle flux dependence on the distance from the plasma. From previous experiments [2] it is known that the proton flux decreases with the distance from the plasma. Due to the better confinement of the lower energy particles in the plasma it is expected that the flux of the 3.0MeV protons is lower than that of the 14.7MeV protons.

The samples were exposed to twelve plasma pulses. The irradiation started the $8^{th}$ of May 2008 14:11 and lasted until 20:49 (UTC). Deuterium was used as fuel for all pulses. In addition, 3He was added from the second to the ninth pulse. The reactions that occurred in the plasma were:

$$D + {}^3He \rightarrow p\ (14.7MeV) + \alpha\ (3.7MeV)$$

$$D + D \rightarrow p\ (3.0MeV) + T\ (1.0MeV)$$

$$D + D \rightarrow n\ (2.5MeV) + {}^3He\ (0.8MeV)$$

$$D + T \rightarrow n\ (14.1MeV) + \alpha\ (3.6MeV)$$

Thus, the possible projectiles to react with the samples were: p (3.0 and 14.7MeV), n (2.5 and 14.1MeV), α (3.6 and 3.7MeV), $^{3}$He (0.8MeV), D (less than 0.1MeV) and T (1.0MeV). At the position of the probe the flux of neutrons is three orders of magnitude higher than the proton flux, thus, neutron induced radionuclides are more likely. Only when there was no neutron induced reaction to produce a certain radionuclide present in a sample, was it possible to ensure that the radionuclide was produced by a proton induced reaction. The flux of the other charged particles was much lower compared with the proton flux.

Shortly after the irradiation, a qualitative gamma-ray analysis of the probe with the samples was performed at the JET site. After six days the samples were shipped to the underground laboratories.

### *2.2. UNDERGROUND LOW-LEVEL GAMMA RAY SPECTROMETRY*

The measurements of the stacked samples were carried out by Institute for Reference Materials and Measurements (IRMM) and Laboratori Nazionali del Gran Sasso (LNGS). The characteristics of the detectors used for the analysis of the nineteen stacked samples are presented in Table 2.

To optimise the efficiency of the measurements the samples were placed in close geometry directly on the detector endcap. For some of the radionuclides this resulted in significant coincidence summing effects (e.g. ~20% for $^{88}$Y) that were taken into account in the Full Energy Peak (FEP) efficiency calculation. These summing effects were calculated at each laboratory using Monte Carlo simulations. The codes used for the calculations were different; EGS4 [7] was used at IRMM and Geant4 [8,9] at LNGS.

### *2.3. IMPURITIES WITH K0-NAA*

From previous experiments it is known that the activation of impurities can explain the presence of certain radionuclides in the samples. For this reason, the impurities of one sample of each type were determined using $k_0$ neutron activation analysis ($k_0$-NAA) at SCK•CEN in Mol [10]. The results of these analyses are presented in Table 3. Most of the major elements in HAVAR could be determined with this technique, however for nickel the detection limit was too high and for this reason the nominal composition, given by the manufacturer, is presented instead. An important trace impurity found in several samples was iron.

### *2.4. PRODUCTION CHANNEL*

The following approach was taken in order to determine the possible reaction channels that produced a certain radionuclide:

i) Look for all the possible reactions considering, as a target, all the isotopes present in the sample (including impurities) and, as a projectile, all the particles present in the plasma. These reactions with their energy thresholds were obtained from [11] which is a website that calculates the Q-values and reaction threshold for all the channels that are possible up to a maximum energy, given in this case by the energy of the particles in the plasma. The

calculation is based on Audi-Wapstra [12] experimental masses when available, otherwise on the FRDM (Finite Range Droplet Model) mass model.

ii) The cross section (CS) for each reaction at the energy of the particle was taken from [13] or [14]. Both websites contain a database for evaluated nuclear data (called Sigma in NNDC and EVA in NEA) and a database of experimental data (called CSISRS in NNDC and EXFOR in NEA). When available the evaluated data is selected. Otherwise, the CS for the reaction is taken from the experimental database. For the experimental values of the CSs, differences were often found for the various references.

iii) A ranking of the most likely reactions for each product was done considering the product of the CS and the amount of the target isotope (all samples had natural isotopic abundances). Since the CS varies with the energy of the particle, this product was calculated for the possible energies of the projectile particle involved.

Table 4 presents an overview of the most likely production channels for the radionuclides found in the different samples. The table displays the CSs at 3.0MeV and at 14.7MeV, the threshold energy, the isotopic abundance and the composition of the target. From this table it is clear that five radionuclides were produced by a proton induced reaction (bold font). The rest all come from neutron induced reactions.

### *2.5. STOPPING POWER AND RANGE*

The aim of using stacked samples was to study the possibility of obtaining information on the relative abundances of 3.0MeV and 14.7MeV protons. This would be possible through the different ranges of protons of different energy. The ranges of protons with 3.0MeV and 14.7MeV for the five different materials of the stacked samples, considering two possible angles of incidence: $90^{o}$ and $45^{o}$, are presented in Table 5. The data was obtained from SRIM (The Stopping and Range of Ions in Matter, [15]). The 3.0MeV protons were stopped in the first sample for all the stacks. For the rhodium and HAVAR stacks it must be noted that they were covered by 0.02mm thick vanadium foils in which most of the energy of the 3.0MeV protons was deposited.

The range of 14.7MeV protons in the samples is of the same order of magnitude as the thickness of the stacks. Thus, the activity of proton induced products is very sensitive to the thickness of the samples. On the other hand, the attenuation of neutrons in matter is very small and for the thickness of the samples is negligible. The activity of neutron induced products remains very uniform along the thickness of the stack. However, for some of the neutron induced products found in the stacked samples a slight non uniformity in the activity distribution has been observed. A similar effect was found for the angular distribution of the neutron flux. In that case it could be explained by an attenuation effect in the sample holder [16]. In the case of the stacks it is not clear yet whether the non uniformity of the neutron flux is due to attenuation, scattering or the combined contribution from several production channels.

## 3. RESULTS

The results, presented in this section, correspond to the proton induced products found in the five stacks. The results are shown in three figures per stack. The first one corresponds to the activity distribution of the proton induced products in the stack. The second figure represents the CS versus depth. The CS of the reactions strongly depends on the energy of the particle, which decreases with the depth. The last figure shows the variation of the energy of the protons as they pass through the stack. This curve was calculated from the values of the stopping power obtained from SRIM. The energy threshold for the proton induced reactions is represented in this last figure with a dashed line.

In principle we expect to have similar profiles in the first and second figures, since the CS expresses the likelihood of interaction between the projectile and the target and the activity quantifies the actual interactions that occurred. The shapes of the second and third figure depend significantly on the angle of incidence of the particles. This angle is unknown, but to estimate the maximum effect that this can have on the reduction of the particle energy along the thickness of the stack, and consequently on the CS in function of the depth of the stack, two possible angles were considered: $90^{o}$ and $45^{o}$.

All activities are given at the reference date 8th of May 2008 at 20:49 (UTC), when the last plasma pulse stopped. The actual activity at the day of measurement was thus lower.

All detection efficiencies were calculated assuming a homogeneous activity distribution of the radionuclide in the sample. Nevertheless, the particle flux depends on the distance to the plasma and thus the activity distribution in the samples may not be uniform. This non-uniform distribution would be specially pronounced in the 40mm long samples (HAVAR, rhodium and yttrium stacks). A discussion about this effect was presented in [5].

The uncertainties are expressed as a combined standard uncertainty following the Guide to the Expression of Uncertainty in Measurements [17].

All the results were compared with the decision threshold (DT), calculated as the upper limit based on a re-normalisation of the statistical distribution around the measured value. The values that were below the DT are presented in figures as a marker without error bars and with the text "DT".

### *3.1 THE YTTRIUM STACK*

The yttrium stack was placed in the sixth slot oriented at 300° with theinternal radius. The samples were 4 cm high with the closest extreme to the plasma placed at 15 mm from the tip of the probe (155 mm away from the outer edge of the plasma).

The five samples were analysed at IRMM in the detectors Ge-6, Ge-4, Ge-3, Ge-8 and Ge-T2. The measurement start date was 15th and 16th of May (1 week after the irradiation) and lasted one day for the samples analysed in the underground laboratory and five days for the sample analysed above ground.

The three radionuclides found in this stack were $^{88}$Y ($T_{½}$ = 107d), $^{89}$Zr ($T_{½}$ = 78h) and $^{182}$Ta ($T_{½}$ =

114 d). The reactions to produce them are presented in Table 4. Yttrium-88 has a main contribution from the neutron induced reaction $^{89}Y(n,2n)^{88}Y$. Considering the difference in flux for neutrons and protons at the position of the probe, the possible contribution of the reaction $^{89}Y(p,n+p)^{88}Y$ is negligible. For $^{89}Zr$ the only production channel is the proton induced reaction $^{89}Y(p,n)^{89}Zr$, which threshold energy is 3.65MeV so only the protons with 14.7MeV can produce it. As can be seen in Table 5 the range of these protons in yttrium for normal incidence is 1.024mm and the total thickness of the stack was 0.75mm, so the protons could pass through the stack.

The activity distribution of $^{88}Y$ and $^{89}Zr$ in the stack is presented in Fig.2, as well as the decrease of energy for the 14.7MeV protons as they pass through the samples and the corresponding CS for the proton induced reaction. The values of the CS for this reaction were taken from the experimental database in NNDC [18-20].

The activity of $^{88}Y$ was quite uniform along the thickness of the stac because the attenuation of neutrons is negligible. This confirms the dominance of the (n,2n) reaction over the (p,n+p) induced reaction. However, a slight descending tendency in the activity along the stack followed by an increase for the last sample is observed. The explanation for this could be, as mentioned before, due to neutron attenuation, neutron scattering or a combined contribution from several production channels. On the other hand, the activity of $^{89}Zr$ decreases as it is expected for a proton induced reaction. As can be seen in Fig.2 the drop of the CS with the energy is reflected in the dependence of the activity with the depth. The decrease of activity with the depth is more pronounced than for the CS, which could indicate that a significant portion of protons arrive at less than normal incidence. For this reason the energy loss and the CS were also calculated at $45^{o}$ and the results are also presented in Fig.2. In this case, the protons that reach the fifth sample in the stack have an energy for which the CS is negligible.

The $^{182}Ta$ found in the samples originated from the tantalum impurities present in the samples (see Table 3) by the reaction $^{181}Ta(n,\gamma)^{182}Ta$. Nevertheless, the high activity measured (~4Bq) indicates that the reaction was mainly produced by neutrons with low energy (<10keV). The CS for this reaction is quite high for low energies but it decreases abruptly for high energies. The values of CS for 3 and 14.7MeV can be found in Table 4.

### *3.2 THE RHODIUM STACK*

The position of the rhodium stack in the probe, at $240^{o}$ with respect to the internal radius, had a smaller proton flux than the samples placed in slots 1, 2 and 6. Furthermore, the stack was covered by a thin vanadium foil (see the range in Table 5).

The four samples were analysed at IRMM in the detectors Ge-6, Ge-8, Ge-3 and Ge-4. The measurements started on the 16th of May, eight days after the irradiation, and lasted four days.

Five radionuclides were detected: $^{102}Rh$ ($T_{½} = 207$ d), $^{102}mRh$ ($T_{½} \sim 2.9$ y), $^{103}Ru$ ($T_{½} = 39.3$ d), $^{103}Pd$ ($T_{½} = 16.991$ d) and $^{192}Ir$ ($T_{½} = 73.8$ d). The five radionuclides that were found in this stack and their possible production reactions are presented in Table 4.

The only proton induced product was $^{103}$Pd. This radionuclide was found in two of the samples in the stack, the second (with an activity of 0.56Bq) and the fourth (with an activity of 0.39Bq). The reason why it was not found in the other two samples is that the energy of the emission X-rays for $^{103}$Pd are between 20.2keV and 23.2keV and were only possible to observe in the detectors with a thin (< 1 μm) deadlayer. Samples 1 and 3 were measured in detectors Ge-6 and Ge-3 respectively which have thicker deadlayers (see Table 3) than detector Ge-8 and Ge-4 where the samples 2 and 4 were measured.

The lower activity found in sample 4 compared to sample 2 indicates that the $^{103}$Pd is mainly produced by a proton induced reaction and the only possible reaction to produce it is $^{103}$Rh(p,n)$^{103}$Pd, which has an energy threshold of 1.34MeV so in principle both protons can produce it. However, the activity for these two samples was surprisingly high, for this reason we considered a possible contribution from a neutron induced reaction. The only neutron induced reactions that produce $^{103}$Pd are: $^{102}$Pd(n,g)$^{103}$Pd, $^{106}$Cd(n,a)$^{103}$Pd, $^{103}$Ag(n,p)$^{103}$Pd and $^{104}$Ag(n,d)$^{103}$Pd. The last two can be discarded since these are not stable isotopes present in natural silver. According to the $k_0$-NAA performed on the rhodium sample, the possible impurities of palladium and cadmium were below decision threshold (< 3mg/kg), furthermore, the isotopic abundance of both isotopes is less than 1.5%. Taking all of this into account, the product of the CS by the maximum possible amount of $^{102}$Pd and $^{106}$Cd is presented in Table 4. As it can be seen the probability of this neutron induced contribution is negligible.

Palladium-103 decays 100% by electron capture to $^{103m}$Rh. The peaks used to determine the activity of 103Pd in the samples were the X-rays of the de-excitation of the daughter nuclei $^{103}$Rh, ($K_{\alpha1} + K_{\alpha2}$: E = 20.1keV, I = 64.7% and $K_{\beta1} + K_{\beta2}$: E = 22.7keV, I = 12.3%). There are other radionuclides that can also contribute to these peaks, such as $^{103}$Ru and $^{103m}$Rh which also emit the same groups of X-ray as $^{103}$Pd. The possible contribution of $^{103m}$Rh originated directly by plasma activation can be discarded because the half life of this radionuclide (56.12m) is much shorter than the time elapsed between irradiation and measurement. Rhuthenium-103 decays by $\beta^-$ to $^{103m}$Rh and $^{103}$Rh but the intensities of the X-rays following this decay are significantly smaller than the intensities of the X-rays following the $^{103}$Pd. However, this contribution was subtracted by determining the activity of $^{103}$Ru with the gamma line at 497 keV. The activity of $^{103}$Ru for the second sample was 32mBq and for the forth 33mBq. Possible contribution of $^{102m}$Rh was also considered. The $K_\alpha$ and $K_\beta$ emission of $^{102m}$Rh are shifted ~1 keV downward with respect to the X-rays of $^{103}$Pd. The activity of $^{102m}$Rh was determined through the gamma lines at 697.49keV and 766.84keV which had no interference with any of the gamma lines of $^{102}$Rh or $^{103}$Ru. The activity of $^{102m}$Rh for the second and forth samples was 13.7mBq and 10.0mBq respectively. The contributions to the 103Pd X-rays from both radionuclides, $^{103}$Ru and $^{102m}$Rh, were rather small (less than 2%). Special attention was also paid to the FEP efficiency calculation at low energies. A correction factor for the efficiency was also calculated using calibrated sources measured in a similar geometry as the sample. The experimental efficiency curve was determined from the following calibrated sources: $^{241}$Am (X-rays

at 17.6keV, 21 keV, 26.34keV and 59.54keV), $^{137}$Cs (32keV, and 36.3keV) and 133Ba (30.8keV, 35keV and 53.16keV). This curve was compared with the simulated curve obtained with EGS4. The ratio of experimental and simulated efficiency was used to correct the simulated efficiency for the $^{103}$Pd X-ray lines. Figure 3 presents the activity of $^{103}$Pd, the CS as function of the depth, and the energy of the 14.7MeV and 3.0MeV protons as they pass through, first the vanadium foil and then the four samples in the stack. As can be seen the CS of the 3.0MeV protons is negligible compared with 14.7MeV protons. The values of the CS were taken from the experimental database in NNDC [21]. As can be seen in the figure, when an incidence angle of 45$^{o}$ is considered the protons are stopped before the last sample in the stack, at approximately 0.26mm depth. However, for this stack was found activity due to $^{103}$Pd in the fourth sample in the stacks indicating that a significant part of the protons arrive with incidence angle greater than 45$^{o}$.

For $^{102}$Rh the main reaction is $^{103}$Rh(n,2n) but there may also be a smaller contribution from the reaction $^{103}$Rh(p,d). However, this contribution must be very small since the distribution of the activity in the stack is very uniform indicating the clear dominance of the neutron induced reaction. The presence of $^{192}$Ir in the samples can be explained by the presence of iridium impurities. An iridium impurity concentration of 63mg/kg was found in the rhodium samples, see Table 3.

### *3.3 THE HAVAR STACK*

The HAVAR stack was placed in the first slot, where the proton flux was at maximum. Like the rhodium stack, it was covered by a vanadium foil of 0.02mm. This material is a commercial cobalt based alloy which composition is presented in Table 3.

The four samples were analysed at LNGS. The measurements started the 21st and 22nd of May, (13 and 14 days after the irradiation) and lasted 13-14 days. Nine radionuclides were detected: $^{59}$Fe ($T_{½}$ = 44.5d), $^{52}$Mn ($T_{½}$ = 5.6 d), $^{54}$Mn ($T_{½}$ = 312.1d), $^{51}$Cr ($T_{½}$ = 27.7d), $^{56}$Co ($T_{½}$ = 77.3d), $^{57}$Co $T_{½}$ = 271.8d), $^{58}$Co ($T_{½}$ = 70.8d), $^{60}$Co ($T_{½}$ = 5.27y) and $^{99}$Mo ($T_{½}$ = 2.7 19d).

Two of the nine radionuclides found in these samples were due to proton activation. These were $^{56}$Co and $^{52}$Mn. Both were detected in the two first samples of the stack and were below the decision threshold for the other two samples. The most likely reaction channels are presented in Table 4. In both cases the threshold energy is greater than 3.0MeV so production can only occur from 14.7MeV protons. The range of such protons in HAVAR is 0.476mm (see Table 5) and the thickness of each sample is 0.2mm.

Figure 4 shows: (on top) the activity distribution of $^{56}$Co and $^{52}$Mn, (in the middle) the CS for both proton induced reactions ($^{52}$Cr(p,n)$^{52}$Mn and $^{56}$Fe(p,n)$^{56}$Co) as function of the depth and (on the bottom) the energy loss of the 14.7MeV protons as they pass through first the vanadium foil and then the four samples in the stack. The dashed line corresponds to the energy threshold which, as can be seen in Table 4, is very similar for both reactions. The last two curves were calculated for two different angles of incidence, 45$^{o}$ and 90$^{o}$. As can be seen in the figure, for normal incidence, the protons were stopped in the third sample in the stack. However, the energy of the protons in the

third sample was below the energy threshold for both reactions so it was not possible to produce the reaction after the 2nd sample. The 45° incidence is also compatible with having activity only in the two first samples of the stack. This agrees with the activity distribution found. The CS curve is very similar for both reactions and the difference in the activity of both radionuclides is due to the shorter half life for $^{52}$Mn and the higher concentration of Cr in the HAVAR alloy (see Table 3).

The values of the CS for both reactions were taken from the experimental database in NNDC [22] for $^{56}$Co and [23] for $^{52}$Mn.

### *3.4 THE BORON CARBIDE STACK*

This stack was placed in the second slot, 160 mm away from the plasma. The thickness of the three samples was different (see Table 1).

The three samples were analysed at IRMM in the detectors Ge-4, Ge-5 and Ge-8. The measurements started on the 27th of May, nineteen days after the irradiation, and lasted two weeks. Only one radionuclide, 7Be (T½= 53.3 d), was detected. The production channel for this radionuclide is presented in Table 4. Both the 3.0 and 14.7 MeV protons can contribute to this reaction.

Figure 5 presents the activity distribution of 7Be in the stack, the CS dependence with the depth for both protons and the energy loss of the 3.0MeV and 14.7MeV protons as they pass through the three samples in the stack. In this case, where it was possible to quantify the contribution to the activity of both protons, it was especially important to determine the effect of the incidence angle in the loss of energy along the thickness of the stack, and the consequent dependence of the CS with the depth. For this reason, the energy loss and the CS were determined for two possible angles of incidence (90° and 45°).

It is clear from Fig.5 that the 3.0MeV protons were completely stopped in the first sample while the 14.7MeV protons with normal incidence passed through the whole stack and the 14.7MeV protons with 45° incidence angle were stopped at a depth of ~0.7mm.

For these samples it was possible to estimate the ratio of 3.0MeV and 14.7MeV. Assuming that the flux of 14.7MeV protons is constant for the two first samples in the stack, the ratio of protons with 3.0MeV and 14.7MeV can be estimated according to this formula:

$$A \propto \sigma \cdot \phi$$

$$\phi_1^{D^3He} \cong \phi_2^{D^3He}$$

$$A_2^{D^3He} = A_2^{Total}$$

$$A_1^{D^3He} = \frac{\sigma_1^{D^3He}}{\sigma_2^{D^3He}} A_2^{D^3He}$$

$$\frac{\phi_1^{DD}}{\phi_1^{D^3He}} = \frac{A_1^{DD}}{A^{D^3He}{}_1} \frac{\sigma_1^{D^3He}}{\sigma_1^{DD}} = \frac{A_1^{Total} - A_1^{D^3He}}{A_1^{D^3He}} \frac{\sigma_1^{D^3He}}{\sigma_1^{DD}} = \frac{A_1^{Total}}{A_1^{D^3He}} - 1 \frac{\sigma_1^{D^3He}}{\sigma_1^{DD}} = \frac{A_1^{Total}}{A_2^{D^3He}} \frac{{}_2^{D^3He}}{{}_1^{D^3He}} - 1 \frac{\sigma_1^{D^3He}}{\sigma_1^{DD}}$$

σ : cross section. For the calculation it has been considered the area under the CS curve for the first

and second sample.

$\phi$: flux

A: activity

The subscript indicates the sample and the superscript the reaction where the protons were generated (D3He for the 14.7MeV protons and DD for the 3.0MeV)

For normal incidence (90°) the activities in the first sample due to the protons with 14.7MeV and 3.0MeV were respectively 2.6(8) mBq and 2.3(11) mBq. The ratio of the 3.0 and 14.7MeV proton flux was: 0.17(10).

For 45° incidence the activities in the first sample due to the protons with 14.7MeV and 3.0MeV were respectively 2.3(7) mBq and 2.7(10) mBq. The ratio of the 3.0 and 14.7MeV proton flux was: 0.31(16).

The CS for this reaction was taken from the evaluated database ENDF/B–VII.0(USA 2006) in [13] and it differs from the values in the experimental database. In addition, it was not possible to find the CS for the reaction, either in [13] or in [14] databases, for energies higher than 10MeV. For this reason, to estimate the ratio of the 3.0MeV and 14.7MeV protons an extrapolation of the CS curve for energies between 10MeV and 14.7MeV was considered.

### *3.5 THE LITHIUM FLUORIDE STACK*

This stack was placed in the second slot, 170mm away from the plasma. As indicated in Table 1, the thickness of the three samples was different. The samples were analysed at IRMM in detectors Ge-3 and Ge-6. The measurements started on the 27th of May and on the 3rd of June, nineteen and twenty-six days after the irradiation. The measurement lasted one week.

Only one radionuclide, $^{7}$Be ($T_{½} = 53.3$d), was detected. Beryllium-7 is a proton induced product (see Table 4). The threshold energy for the reaction $^{7}$Li(p,n)$^{7}$Be is 1.88MeV, so in principle, both the 3.0MeV and the 14.7MeV protons can contribute to this reaction.

Figure 6 presents the activity distribution of $^{7}$Be, the CS dependence with the depth for the 3.0MeV and 14.7MeV protons and for two incidence angles (90° and 45°) and the energy loss for both protons and both angles of incidence. The CS for this reaction was taken from the experimental database in NEA [24] and it differs from the values of the evaluated data from NNDC.

As in the case of $B_4C$, the 3.0MeV protons were completely stopped in the first sample, no matter the angle of incidence. The 14.7MeV protons which came with an incident angle of 90° passed through the whole stack while the ones with 45° incidence angle were completely stopped in the third sample, at about 0.8mm depth. The CS for this reaction has a maximum for low energies. Thus, there is a significant dependence of the CS for the 14.7MeV protons in the third sample with the angle of incidence.

The activity contribution of the 3.0MeV and 14.7MeV protons to the activity in the first sample and the flux of both protons was calculated as it is described in the previous section. The result obtained was that, within the uncertainty, there was no contribution from the 3.0MeV protons.

This means that, as was expected, the flux for the 3.0MeV protons at the position of the sample is significantly lower than for the 14.7MeV and the activity induced by the 3.0MeV protons can be neglected.

The LiF sample placed in the same slot as the LiF stack but further from the plasma (see Fig.1) was analysed with the GeCris detector. The measurement started 91 days after the irradiation and lasted for two weeks. This sample had a thickness of 1 mm and an activity of 1.2(6)mBq which is significantly lower than the activity in the first sample of the stack (8.6(16) mBq). This confirms the fact that the proton flux decreases considerably with the distance to the plasma.

## 4. DISCUSSION

The results obtained for the $B_4C$ and LiF stacks, where the threshold energy for (p,a) and (p,n) reactions respectively is below 3. MeV and thus both protons can contribute to the production of 7Be, show that it is possible to differentiate the 3.0MeV and the 14.7MeV protons from the D-D and the D-3He fusion reactions respectively. In the case of the B4C stack, the ratio of the 3.0MeV and 14.7 MeV protons could be quantified at the position of the stack. For the LiF stack, which was placed further away from the plasma than the B4C stack, the results indicate no significant activation due to 3.0 MeV protons. This could be explained due to the sharp reduction of the particle flux with the distance to the plasma. The lower flux of 3.0 MeV protons compared to the 14.7 MeV proton flux is in agreement with the expectation that lower energy protons are better confined in the fusion plasma than higher energy protons.

In order to improve this technique to quantify the ratio of 3.0MeV and 14.7MeV protons at a certain position of the probe it would be necessary to better know the angle of incidence of the detected protons. This could be achieved e.g through the use of a collimated stack to accept only protons entering a small solid angle. A better knowledge of the CS for the proton induced reactions would also reduce the uncertainty of the ratio.

Our study shows the sensitivity of the results to the angle of incidence of the charged particles. The results for the high energy protons clearly suggest, for the stacks in slot 2 and 6, an averaged angle of incidence for the protons which is lower than the normal incidence (90°). For the HAVAR stack in slot 1, a normal averaged incidence angle for the protons is compatible with the distribution of the activity in the stack. These results are in agreement with the preliminary modelling of the trajectories of the fusion protons.

In all the materials considered for this study proton induced radionuclides have been found. In order to determine which materials and reactions are best suited to study the leakage and distribution of protons there are several things to consider. The main goal is to have a reaction with a high production yield, and thus high activity. The production yield depends on: i) the CS, ii) the isotopic abundance, iii) the atomic fraction in compounds and iv) the energy threshold. From the point of view of gamma spectrometry there are also some aspects to take into account for choosing a suitable reaction: i) half life, ii) emission probability, iii) gamma-ray energies, and iv) coincidence

summing effects. There are no materials or reactions that meet all the above mentioned requisites. It is necessary to find a compromise to choose the best suitable samples for future experiments.

The fact that $^{103}$Pd activity has been measured for two of the samples proves that $^{103}$Rh(p,n)$^{103}$Pd may be a suitable reaction to study the 14.7MeV protons. However, it would be necessary to use detectors with thin deadlayer to be able to detect the low energy peaks. It would be very interesting for future experiments to measure the $^{103}$Pd activity in all the samples in the stack. This would confirm the values obtained in this experiment, which are surprisingly high, especially for the last sample in the stack. In addition, the activity distribution across the stack could provide useful information on the angle of incidence e.g. only for normal incidence would it be possible to have $^{103}$Pd in the last sample of the stack (see CS distribution in Fig.3). This fact, together with the high activity found in the fourth sample of the stack, lead us to think of a possible mistake in the labelling of the samples (which we found no other indication of) or another possible contribution, different than $^{103}$Pd, to the X-ray peaks analysed (20keV and 22keV). A possible way of confirming this is determining the half life by measuring one sample for several days and analysing the activity decay. Unfortunately none of the rhodium samples were measured for enough time to do that. We consider that it would be veryinteresting to include again a rhodium stack in future experiments to clarify all of these points.

Another radionuclide which had high activity was the $^{89}$Zr found in the yttrium stack. The half life of this radionuclide (78 h) is long enough to measure the activity after the irradiation. There is only one gamma-ray with emission probability high enough to be measured (909keV I = 99%) but it is in a favourable region of the spectrum with low background and no interference from other radionuclides.

Regarding the HAVAR stack one of the advantages is that two proton induced products were found ($^{56}$Co and $^{52}$Mn), but, because of the atomic fraction of iron and chromium in HAVAR, the activities were not as high as for $^{103}$Pd and $^{89}$Zr. However, the activity of both radionuclides could be determined through more than one gamma-ray (For $^{56}$Co: 846.76keV (I = 99.9%) and 1238keV (I = 66.8%) and for $^{52}$Mn: 744.2keV (I = 90%), 935.5 (I = 95%) and 1434keV (I = 99.9%)). This reduces the uncertainty of the activity calculation. The drawback for this stack was the short range of protons that could only induce the reactions for the two first samples in the stack. In case this material will be used in future experiments it would be preferable to have thinner samples in the stack in order to obtain information of the angle of incidence and the activity distribution.

The activity of $^{7}$Be found in both LiF and $B_4C$ stacks was rather low. However, they were the only two materials where the study of the 3 MeV protons could be done. The main reasons for the low activity are the isotopic abundance (19.9% for 10B and 92.4% for $^{7}$Li), the mass percentage of target element in the sample (78.26% of B in $B_4C$ and 73.24% of F in LiF) and the low emission probability of the only gamma ray in $^{7}$Be (10.44%). The main limitation to the study of the 3MeV and 14.7MeV protons ratio is the position of the stack in the sample holder. Since the attenuation of the proton flux with the distance to the plasma is very pronounced, it is necessary to have the samples as close as possible to the plasma.

A general difficulty for the analysis of the distribution of the proton induced products in the stacks was due to the lack of knowledge of the CS for many of the reactions. The experimental data was not always in agreement with each other and the available range of energies did not always cover the needs for this study (between 0 and 14.7MeV). This introduces an additional source of uncertainty for the determination of the ratio of 3MeV and 14.7MeV protons together with the lack of knowledge of the angle of incidence.

It is not the aim of this article to study the neutron induced products in the stacks but it is worth pointing out that several of them had a slight non uniform distribution. In this article the example of $^{88}$Y was briefly mentioned but it was not the only one. It would be interesting for further experiments to study this effect.

## CONCLUSIONS

The main objectives of the experiment were achieved:

- Proton induced products were found in all five stacks.
- For the first time the ratio of 3MeV and 14.7MeV protons was experimentally determined.
- It has been confirmed that the flux of 14.7MeV protons is larger that the flux of 3MeV protons which is expected from the confinement of protons in plasma.
- In addition, some information about the angle of incidence and theattenuation of the proton flux with the position of the samples was 3 obtained.
- The activity distribution in the stacks placed in the slots 2 and 6 was due to protons arriving at incidence angle less than 90$^{o}$ which is expected from the calculation of the proton trajectories.

There are however certain aspects of the experiment that can be improved in future experiments:

- The use of more detectors with thin deadlayers may allow measuring all the samples in the rhodium stack and may allow the determination not only of the 103Pd activity in all the samples but also the half life, to ensure that the analysed peaks correspond to this radionuclide.
- Information about the angle of incidence that could have been obtained for the HAVAR stack has been hampered due to the thickness of the samples and the range of the 14.7MeV protons. Cobalt-56 and $^{52}$Mn were only found in the first two samples of the stack and this is compatible with a wide range of angles of incidence, from 45$^{o}$ to 90$^{o}$.
- In order to reduce the uncertainty due to the not very well known angle of incidence it would be interesting to develop more detailed models of the trajectories of the particles inside the Tokamak. Another possibility would be to modify the experimental setup to have collimated stacks where only the protons with a fixed incidence angle can reach the samples.
- A better knowledge of the angle of incidence and an adequate placement of the samples, close to the plasma, may improve the determination of the 3MeV and 14.7MeV protons and give information about the concentration of the fusion fuel in the plasma (D/$^{3}$He).

**ACKNOWLEDGEMENTS**

The work done by EURIDICE and the HADES team of SCK•CEN in Mol, Belgium, is gratefully acknowledged. This work was supported by EURATOM and carried out within the framework of the European Fusion Development Agreement. The views and opinions expressed herein do not necessarily reflect those of the European Commission.

**REFERENCES**

[1]. Gasparro, J., et al., A low-level activation technique for monitoring thermonuclear fusion plasma conditions. Applied Radiation and Isotopes, 2006. **64**(10-11): p. 1130-1135.

[2]. Wieslander, J.S.E., et al., Low-level gamma-ray spectrometry for analysing fusion plasma conditions. Nuclear Instruments and Methods in Physics Research A, 2008. 591: p. **383-393**.

[3]. Bonheure, G., et al., Measurements of MeV particles from JET fusion plasmas based on the activation technique. Physica Scripta, 2007. **75**: p. 769-773.

[4]. Bonheure G., et al., Mega-electron-volt ion loss measurements in JET D-3He plasmas using activation technique. Fusion Science and Technology, 2008. **53**(3): p.806-815.

[5]. González de Orduña, R., et al., Angular distribution of proton leakage from a fusion plasma using ultra low-level gamma-ray spectrometry. Applied Radiation and Isotopes, 2009. **68**(7-8): p. 1226-1230.

[6]. Bonheure, G., et al., Charged fusion product loss measurements using nuclear activation analysis. Review of Scientific Instruments 2010. **81**(10).

[7]. Nelson, W.R., H. Hirayama, and D.W.O. Rogers, The EGS4 code system, S.-R. 265, Editor. 1985, Stanford Linear Accelerator Centre: Stanford, California.

[8]. Agostinelli, S., et al., Geant4 - a simulation toolkit. Nuclear Instruments and Methods in Physics Research Section A, 2003. **506**(3): p. 250-303.

[9]. Allison, J., et. al., Geant4 developments and applications. IEEE Transactions on Nuclear Science, 2006. **53**(1): p. 270-278.

[10]. Etxebarria, N., et al., Proceedings of the Second International k0-Users Workshop, Ljubljana, Slovenia, 1996. p. 137-141.

[11]. Qtool: Calculation of Reaction Q-values and Thresholds. http://t2.lanl.gov/data/qtool.html, 1997.

[12]. Audi, G. and A.H. Wapstra, The 1993 atomic mass evaluation: (I) Atomic mass table. Nuclear Physics A, 1993. **565**(1): p. 1-65.

[13]. National Nuclear Data Center. http://www.nndc.bnl.gov/.

[14]. Nuclear Energy Agency. http://www.nea.fr/.

[15]. The Stopping and Range of Ions in Matter. http://www.srim.org/.

[16]. Bonheure G., et al., In-vessel activation monitors in JET: Progress in modeling. Review of Scientific Instruments, 2008. **79**(10).

[17]. ISO/IEC/OIML/BIPM, Guide to the Expression of Uncertainty in Measurement. 1995, International Organization for Standardization: Geneva, Switzerland.

[18]. Johnson, C.H., R.L. Kernell, and S. Ramavataram, The 89Y(p,n)89Zr cross section near the first two analogue resonances. Nuclear Physics A, 1968. 107: p. 21.

[19]. Albert, R.D., (p,n) cross section and proton optical-model parameters in the 4 to 5.5MeV energy region. Physical Review 1959. 115: p. 925.

[20]. Wenrong, Z., et al., Investigation of Y-89(p,n)Zr-89, Y-89(p,2n)Zr-88 and Y-89(p,pn)Y-88 reactions up to 22MeV. Chinese J. of Nuclear Physics, 1990. **14**(1): p. 7.

[21]. Sudár, S., F. Cserpák, and S.M. Qaim, Measurements and nuclear model calculations on proton-induced reactions on 103Rh up to 40 MeV: evaluation of the excitation function of the 103Rh(p,n)103Pd reaction relevant to the production of the therapeutic radionuclide 103Pd. Applied Radiation and Isotopes, 2002. **56**(6): p.821-831.

[22]. Wenrong, Z., L. Hanlin, and Y. Weixiang, Measurement of cross sections by bombarding Fe with protons up to 19 MeV. Chinese J. of Nuclear Physics, 1993. **15**(4): p. 337.

[23]. Tanaka, S. and M. Furukawa, Excitation functions for (P,N) reactions with titanium, vanadium, chromium, iron and nickel up to 14MeV. Physical Society of Japan, 1959. 14: p. 1269.

[24]. Abramovich S.N., et al., Estimated values of total and differential cross sections of proton interactions with nuclei Li-6 and Li-7. Vop. At.Nauki i Tekhn.,Ser.Yadernye Konstanty,, 1984( Issue.4,): p.17

| | | Position in the stack | | | | |
|---|---|---|---|---|---|---|
| | | 1 | 2 | 3 | 4 | 5 |
| Y stack | Thickness (mm) | 0.14(1) | 0.14(1) | 0.14(1) | 0.14(1) | 0.14(1) |
| | Mass (g) | 0.252(1) | 0.248(1) | 0.252(1) | 0.250(1) | 0.251(1) |
| | Length (cm) | 4.0(1) | 4.0(1) | 4.0(1) | 4.0(1) | 4.0(1) |
| HAVAR stack | Thickness (mm) | 0.20(1) | 0.20(1) | 0.20(1) | 0.20(1) | - |
| | Mass (g) | 0.70(1) | 0.68(1) | 0.68(1) | 0.68(1) | - |
| | Length (cm) | 4.0(1) | 4.0(1) | 4.0(1) | 4.0(1) | |
| Rh stack | Thickness (mm) | 0.10(1) | 0.10(1) | 0.10(1) | 0.10(1) | - |
| | Mass (g) | 0.515(1) | 0.518(1) | 0.517(1) | 0.511(1) | - |
| | Length (cm) | 4.0(1) | 4.0(1) | 4.0(1) | 4.0(1) | |
| LiF stack | Thickness (mm) | 0.26(1) | 0.26(1) | 0.43(1) | - | - |
| | Mass (g) | 0.071(1) | 0.069(1) | 0.113(1) | - | - |
| | Length (cm) | 1.0(1) | 1.0(1) | 1.0(1) | | |
| $B_4C$ stack | Thickness (mm) | 0.22(1) | 0.18(1) | 0.51(1) | - | - |
| | Mass (g) | 0.054(1) | 0.045(1) | 0.127(1) | - | - |
| | Length (cm) | 1.0(1) | 1.0(1) | 1.0(1) | | |

*Table 1: Characteristics of the samples in the stacks. (Position 1 corresponds to the outer sample in the stack).*

| | Location | Type | Mass (g) | A.V[a] ($cm^3$) | R.E[b] (%) | Window (thickness) | T.D.L[c] (cm) |
|---|---|---|---|---|---|---|---|
| Ge-3 | IRMM (HADES) | Coaxial | 1337 | 225.4 | 60 | LB-AL 0.7 mm | 0.085 |
| Ge-4 | IRMM (HADES) | Coaxial (XtRa) | 2186 | 410.6 | 103.1 | LB-AL 1.5 mm | $5\ 10^{-5}$ |
| Ge-6 | IRMM (HADES) | Coaxial | 2104 | 395.2 | 80.5 | Cu 1 mm | 0.09 |
| Ge-8 | IRMM (HADES) | Planar (BEGe) | 76.9 | 12.38 | 19 | LB-AL 1.5 mm | $3\ 10^{-5}$ |
| Ge-5 | IRMM (HADES) | Planar (BEGe) | 825 | 143.2 | 50 | LB-AL 1.5 mm | $2\ 10^{-4}$ |
| Ge-T2 | IRMM | Coaxial | 454 | 71.31 | 19.6 | LB-AL | 0.075 |
| GeCris | LNGS | Coaxial p | 2470 | 465 | 120 | Cu 1mm | 0.1 |
| GeBer | LNGS | Coaxial n | 1250 | 235 | 54 | Carbon fibre 0.76 mm | $3\ 10^{-5}$ |
| GeMi | LNGS | Coaxial p | 2200 | 414 | 86 | Cu 0.5 mm | 0.15 |
| GePV | LNGS | Coaxial p | 1940 | 363 | 91 | Cu 2 mm | 0.15 |
| GePaolo | LNGS | Coaxial p | 2760 | 518 | 113 | Cu 2 mm | 0.15 |

[a] A.V: Active volume
[b] R.E: Relative efficiency
[c] T.D.L: Top DeadLayer

*Table 2: Characteristics of the HPGe detectors used for measuring the stacked samples.*

| **Impurity** | **Y** | **HAVAR** | **Rh** | **LiF** | **$B_4C$** |
|---|---|---|---|---|---|
| Gd | 130(20) | - | - | - | - |
| Ho | 35(2) | - | - | - | - |
| Ta | 0.71(5)% | - | - | - | - |
| Co | - | 40(2)% | - | - | 0.23(7) |
| Fe | - | 16.9(9)% | 110(20) | 27(10) | 600(180) |
| Cr | - | 19.5(10)% | 8(3) | - | 10(3) |
| Ni | - | 13%* | - | - | - |
| Mo | - | 2.4(2)% | - | - | - |
| Mn | - | 1.54(8)% | - | - | - |
| W | - | 2.7(2)% | - | - | - |
| Ru | - | - | 19(2) | - | - |
| Ir | - | - | 63(6) | - | - |
| Sb | 1.0(2) | - | 0.23(4) | 0.011(5) | - |

* This element could not be determined by $k^0$-NAA so the nominal composition, given by the manufacturer, is given instead.

*Table 3: Impurities and major constituents for the various stacked material detected using $k_0$-NAA. The unit is mg/kg except when % sign is given. The uncertainty in brackets is the expanded uncertainty, with k=2 and relates to the last significant digit.*

| S[a] | RN[b] | PR[c] | CS[d] (b) @ 3 MeV | CS (b) @ 14 MeV | Thr[e] (MeV) | IA[f] (%) | C[g] (%) | CS*IA*C @ 3 MeV (%) | CS*IA*C @ 14 MeV (%) |
|---|---|---|---|---|---|---|---|---|---|
| $B_4C$ | **$^{7}$Be** | **$^{10}$B(p,α)$^{7}$Be** | 0.095 | - | 0 | 19.9 | 78.26 | 1.5 | - |
| LiF | **$^{7}$Be** | **$^{7}$Li(p,n)$^{7}$Be** | 0.25 | 0.03 | 1.9 | 92.4 | 73.24 | 17.0 | 1.8 |
| | | $^{6}$Li($^{3}$He,d)$^{7}$Be | $4.4\cdot10^{-3}$ * | - | 0 | 7.6 | 73.24 | 0.02 | - |
| | | $^{6}$Li(d,n)$^{7}$Be | $6.3\cdot10^{-4}$ * | - | 0 | 7.6 | 73.24 | 0.00 | - |
| Y | $^{88}$Y | $^{89}$Y(n,2n)$^{88}$Y | - | 0.82 | 11.6 | 100 | 100 | - | 82.4 |
| | | $^{89}$Y(γ,n)$^{88}$Y | - | 0.02 | 11.5 | 100 | 100 | - | 2.4 |
| | | $^{89}$Y(p,n+p)$^{88}$Y | - | $1.2\cdot10^{-3}$ | 11.6 | 100 | 100 | - | 0.12 |
| | $^{182}$Ta | $^{181}$Ta(n,γ)$^{182}$Ta | $2.8\cdot10^{-2}$ | $4.9\cdot10^{-3}$ | 0 | 100 | 0.71 | 0.02 | 0.003 |
| | **$^{89}$Zr** | **$^{89}$Y(p,n)$^{89}$Zr** | $4.7\cdot10^{-4}$ | 0.7 | 3.7 | 100 | 100 | 0.05 | 74 |
| Rh | $^{102}$Rh | $^{103}$Rh(n,2n)$^{102}$Rh | - | 1.3 | 9.4 | 100 | 100 | - | 128 |
| | | $^{103}$Rh(p,d)$^{102}$Rh | - | 0.7 | 7.2 | 100 | 100 | - | 70.0 |
| | $^{103}$Ru | $^{103}$Rh(n,p)$^{103}$Ru | $3.2\cdot10^{-5}$ | $2.1\cdot10^{-2}$ | 0 | 100 | 100 | 0.00 | 2.1 |
| | **$^{103}$Pd** | **$^{103}$Rh(p,n)$^{103}$Pd** | $2.8\cdot10^{-4}$ | 0.11 | 1.3 | 100 | 100 | 0.03 | 11.0 |
| | $^{103}$Pd | $^{102}$Pd(n,γ)$^{103}$Pd | $9.5\cdot10^{-2}$ | $7.2\cdot10^{-3}$ | 0.0 | 1.02 | $<3\cdot10^{-4}$ | $<2.9\cdot10^{-7}$ | $<2.2\cdot10^{-8}$ |
| | $^{103}$Pd | $^{106}$Cd(n,α)$^{103}$Pd | $6.6\cdot10^{-3}$ | $1.0\cdot10^{-1}$ | 0.0 | 1.25 | $<3\cdot10^{-4}$ | $<2.5\cdot10^{-8}$ | $<3.8\cdot10^{-7}$ |
| | $^{192}$Ir | $^{193}$Ir(n,2n)$^{192}$Ir | - | 2.1 | 7.8 | 62.7 | $6.3\cdot10^{-3}$ | - | 0.01 |
| HAVAR | $^{59}$Fe | $^{59}$Co(n,p)$^{59}$Fe | $3.3\cdot10^{-4}$ | $5.0\cdot10^{-2}$ | 0.8 | 100 | 40 | 0.01 | 2.0 |
| | | $^{62}$Ni(n,α)$^{59}$Fe | $2\cdot10^{-4}$ | 0.02 | 0.4 | 3.63 | 12 | 0.00 | $9\ 10^{-3}$ |
| | **$^{52}$Mn** | **$^{52}$Cr(p,n)$^{52}$Mn** | - | 0.26 | 5.6 | 84 | 20 | - | 4.3 |
| | | $^{54}$Fe(n,t)$^{52}$Mn | - | $7.5\cdot10^{-5}$ | 12.7 | 6 | 17 | - | 0.0 |
| | $^{54}$Mn | $^{54}$Fe(n,p)$^{54}$Mn | 0.15 | $3.4\cdot10^{-1}$ | 0 | 5.8 | 16.9 | 0.15 | 0.3 |
| | | $^{54}$Cr(p,n)$^{54}$Mn | $3.7\cdot10^{-2}$ | 0.5 | 2.2 | 2.4 | 19.5 | 0.02 | 0.2 |
| | $^{51}$Cr | $^{52}$Cr(n,2n)$^{51}$Cr | - | 0.23 | 12.3 | 83.8 | 20 | - | 3.8 |
| | | $^{54}$Fe(n,α)$^{51}$Cr | $1.8\cdot10^{-5}$ | 0.08 | 0 | 5.8 | 17 | 0.00 | 0.08 |
| | **$^{56}$Co** | **$^{56}$Fe(p,n)$^{56}$Co** | - | 0.36 | 5.4 | 91.7 | 16.9 | - | 5.5 |
| | | **$^{57}$Fe(p,2n)$^{56}$Co** | - | 0.01 | 13.2 | 2.2 | 16.9 | - | 0.0 |
| | | $^{58}$Ni(n,t)$^{56}$Co | - | $1.2\cdot10^{-5}$ | 11.3 | 68.1 | 12.0 | - | 0.0 |
| | $^{57}$Co | $^{58}$Ni(n,n+p)$^{57}$Co | - | 0.55 | 8.3 | 68.1 | 12.0 | - | 4.5 |
| | | $^{58}$Ni(p,2p)$^{57}$Co | - | 0.16 | 8.3 | 68.1 | 12.0 | - | 1.3 |
| | | $^{60}$Ni(p,α)$^{57}$Co | <0.001 | 0.09 | 0.27 | 26.2 | 12.0 | 0.00 | 0.3 |
| | $^{58}$Co | $^{59}$Co(n,2n)$^{58}$Co | - | 0.6 | 10.6 | 100 | 40.0 | - | 24 |
| | | $^{58}$Ni(n,p)$^{58}$Co | 0.18 | 0.44 | 0 | 68.1 | 12.0 | 1.45 | 3.6 |
| | | $^{59}$Co(p,n+p)$^{58}$Co | - | 0.04 | 10.6 | 100 | 40.0 | - | 1.6 |
| | $^{60}$Co | $^{59}$Co(n,γ)$^{60}$Co | $2.2\cdot10^{-3}$ | $7.8\cdot10^{-4}$ | 0 | 100 | 40.0 | 0.09 | 0.03 |
| | $^{99}$Mo | $^{100}$Mo(n,2n)$^{99}$Mo | - | 1.49 | 8.4 | 9.63 | 2.4 | - | 0.3 |

[a] S: Sample
[b] RN: Radionuclide found
[c] PR: Production reaction
[d] CS: Cross section
[e] Thr: Energy threshold for the reaction
[f] IA: Isotopic Abundance
[g] C: mass percentage of the target element present in the sample.
* This cross section is for the maximum energy of the particle involved (0.1 MeV for d and 0.8 MeV$^{3}$ for He)

*Table 4: Overview of the likely production reaction channels for the radionuclides found in the 5 stacks.*

| Sample | 3 MeV 90° | 14.7 MeV 90° | 3 MeV 45° | 14.7 MeV 45° | Sample Thickness (mm) |
|---|---|---|---|---|---|
| $B_4C$ | 0.063 | 1.024 | 0.046 | 0.7 | 0.9 (0.22+0.18+0.51) |
| LiF | 0.072 | 1.158 | 0.052 | 0.8 | 0.8 (0.26+0.26+0.43) |
| Y | 0.077 | 1.024 | 0.056 | 0.7 | 0.75 (0.14 ×5) |
| HAVAR* | 0.034 | 0.476 | 0.026 | 0.3 | 0.8 (0.2 ×4) |
| Rh* | 0.029 | 0.377 | 0.009 | 0.3 | 0.4 (0.1 ×4) |
| V | 0.045 | 0.654 | 0.03 | 0.5 | 0.02 |

*HAVAR and Rh stacks were covered by a vanadium foil

*Table 5: Range in mm for 3.0MeV and 14.7MeV protons, obtained from SRIM considering normal incidence and 45°.*

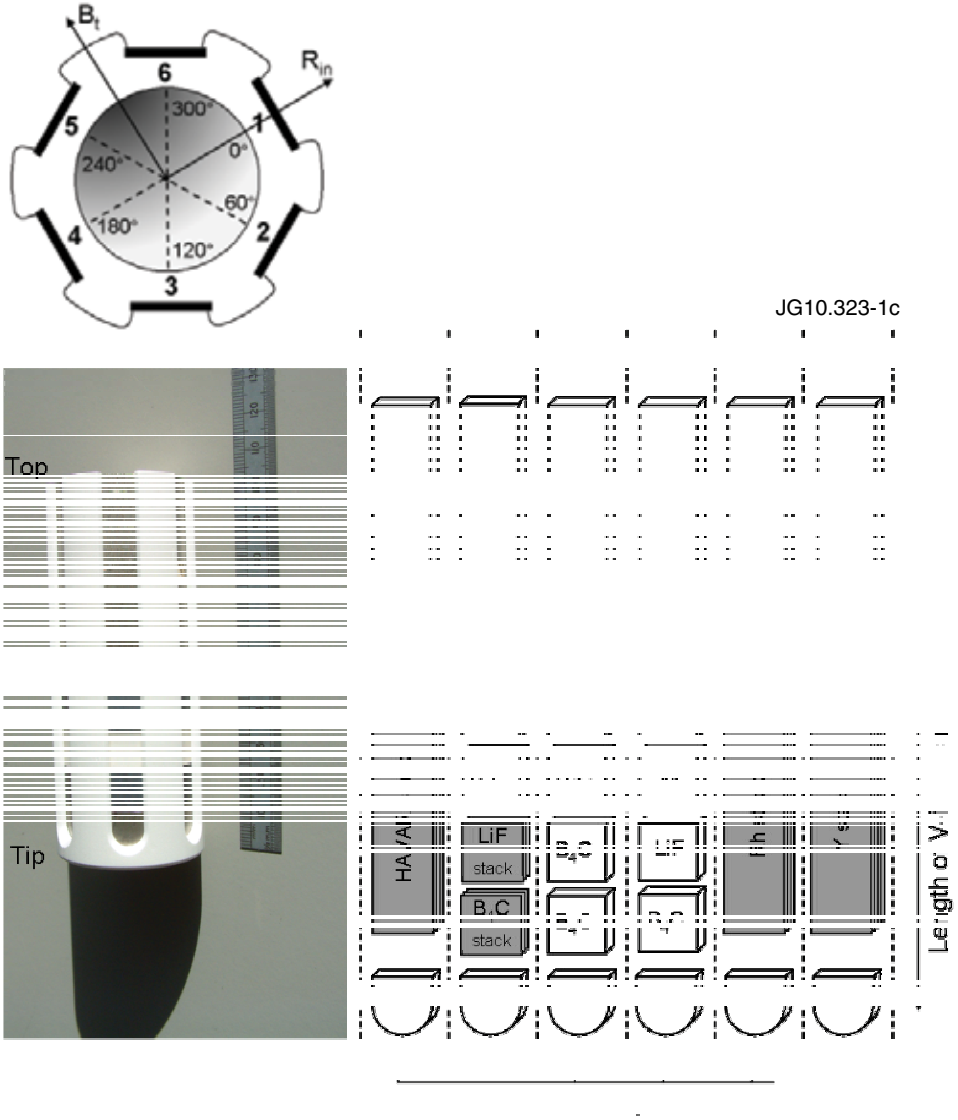


*Figure 1: (a) Cross section of the probe and its orientation with respect to the toroidal magnetic field ($B_t$) and the major radius of the tokamak ($R_{in}$), (b) picture of the BN activation probe and (c) schematic diagram of the sample layout. The numbers in (a) and (c) indicate the six slots where the samples were placed.*

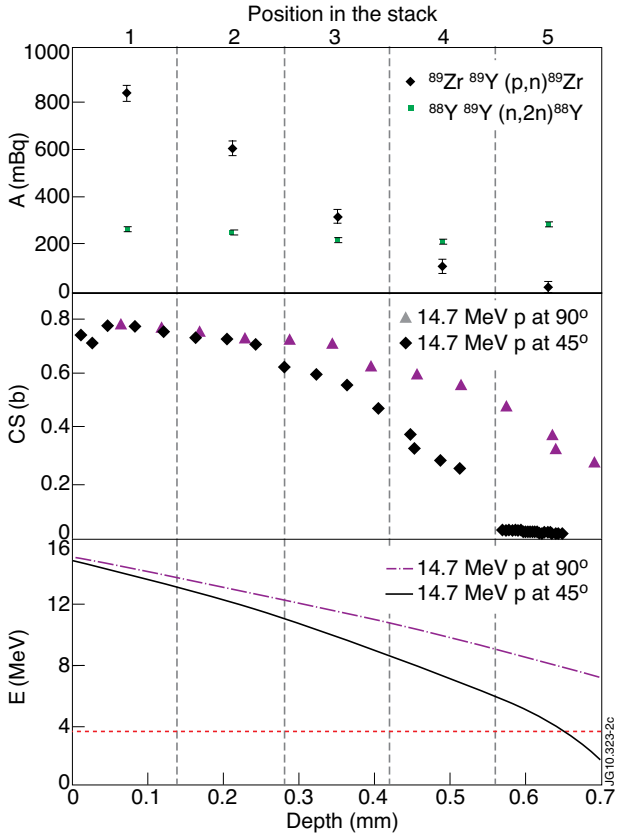


*Figure 2: Data for the yttrium stack. The bottom curve shows the energy of 14.7MeV protons as they traverse the stack (at normal incidence and for 45° incidence). The dashed line corresponds to the energy threshold of the proton induced reaction. The middle curve shows the CS as function of the depth in the stack (at normal incidence and for 45° incidence). The top curve shows the activity of the radionuclides found in the stack.*

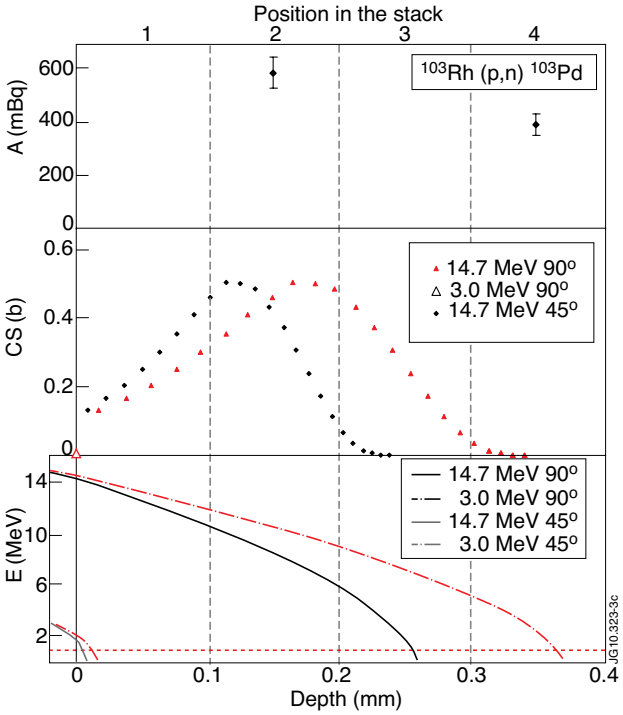


*Figure 3: As Figure 2 but for the rhodium stack. In the bottom curve the part below 0 corresponds to the vanadium foil that was covering the stack.*

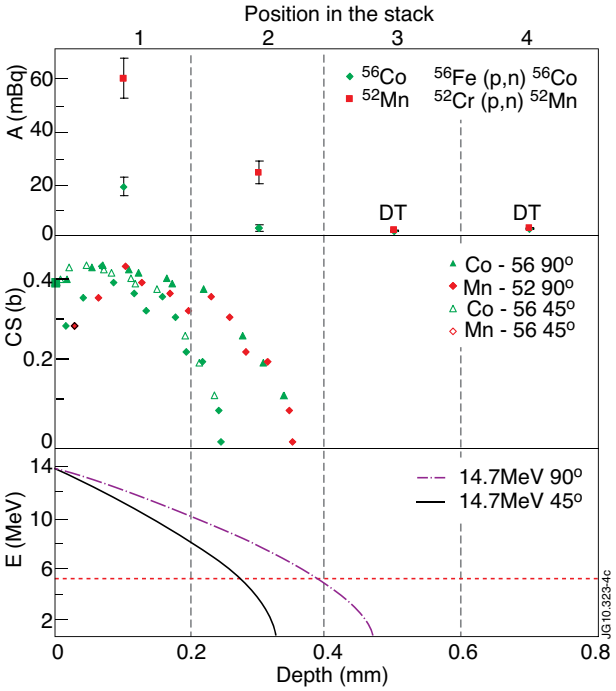


*Figure 4: As Figure 2 but for the HAVAR stack.*

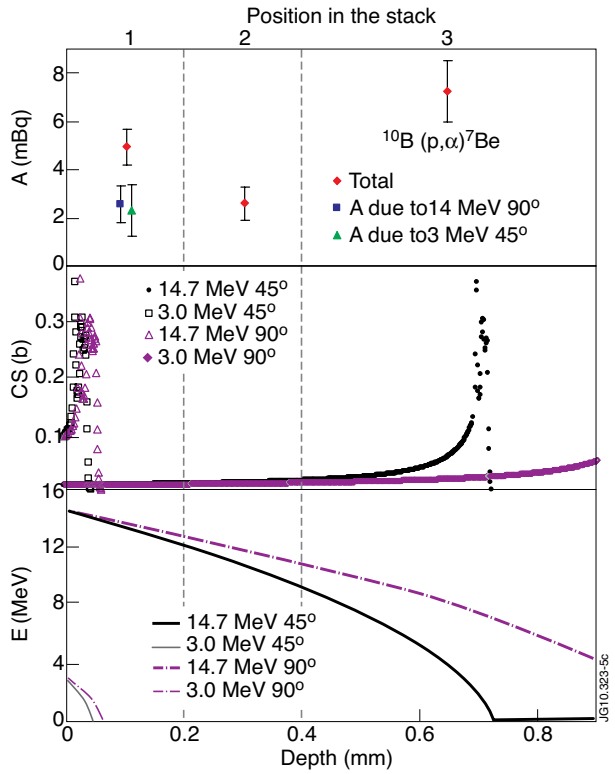


*Figure 5: As Figure 2 but for the LiF stack.*

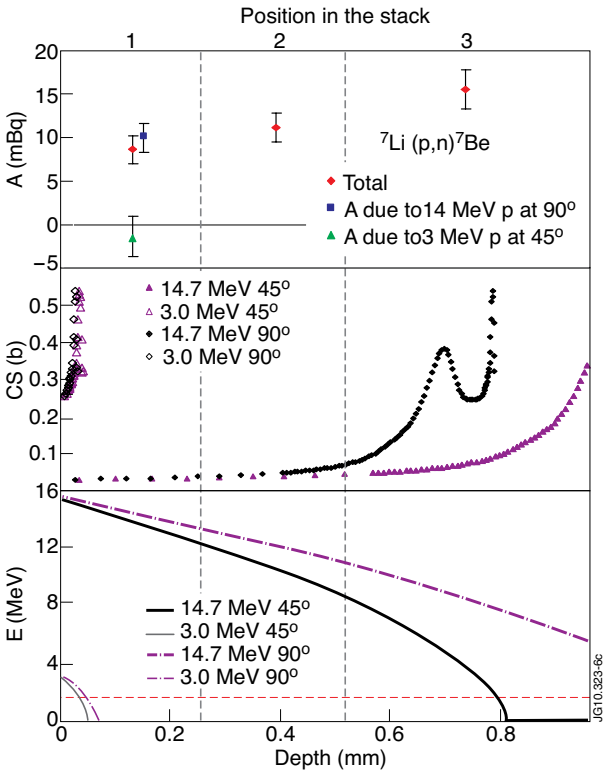


*Figure 6: As Figure 2 but for the $B_4C$ stack.*